RECENT X-RAY OBSERVATIONS AND THE EVOLUTION OF HOT GAS IN ELLIPTICAL GALAXIES: EVIDENCE FOR CIRCUMGALACTIC GAS[1]

Fabrizio Brighenti[2,3] and William G. Mathews[3]

[2]*Dipartimento di Astronomia, Università di Bologna, via Zamboni 33, Bologna 40126, Italy*
brighenti@astbo3.bo.astro.it

[3]*University of California Observatories/Lick Observatory, Board of Studies in Astronomy and Astrophysics, University of California, Santa Cruz, CA 95064*
mathews@lick.ucsc.edu

Abstract

The radial variation of hot gas density and temperature in bright elliptical galaxies provided by x-ray observations can be used to accurately determine the radial distribution of total galactic mass using the condition of hydrostatic equilibrium. However, we set out here to solve the inverse problem. Starting with the known distributions of total mass and mass-losing stars in a specific large elliptical, NGC 4472, we attempt to solve the gas dynamical equations to recover the currently observed radial distribution of density and temperature in the hot interstellar gas. The galaxy is assumed to be initially gas-free as a result of early SNII-driven galactic winds. In seeking this agreement we consider a variety of assumptions for the evolution of the hot interstellar gas: mass dropout, variation of stellar mass loss with galactic radius, variation of the bolometric radiative cooling rate with galactic radius, and several supernova rates. After evolving for a Hubble time, none of these models accounts for several well-observed properties of the interstellar gas: gas temperatures that significantly exceed the mean stellar temperatures, positive temperature gradients within a few effective radii, shallow density gradients, and large interstellar gas masses.

However, all of these discrepancies are lessened or disappear if large masses of hot gas are assumed to be present in the outer galactic potential at early times in galactic history. Most of the interstellar mass that contributes to cooling flows in galaxies like NGC 4472 has not come from mass lost by galactic stars since ~ 1 Gyr. The sustained inflow of hot gas from this circumgalactic environment may help to resolve other long-standing problems that have beset models of galactic cooling flows: the wide range of L_x/L_B for fixed L_B; the variable and often low iron abundances observed in ellipticals, and the failure (so far) to observe pronounced rotational flattening in x-ray images of slowly rotating giant ellipticals.

The characteristic hot gas temperature profile observed in many bright ellipticals has a maximum at $\sim 3\ r_e$. This can be understood as the mixing of gas ejected from stars with old circumgalactic gas flowing in from the halo. Since the circumgalactic gas is hotter than the stars, mass dropout is not needed to flatten the gas density gradient. Moreover, the agreement of the stellar mass in NGC 4472 (and NGC 4649) within r_e determined from stellar dynamics with the total mass determined by hot gas hydrostatic equilibrium is an additional argument against mass dropout.

Subject headings: galaxies: elliptical and lenticular — galaxies: cooling flows – X-rays: galaxies

1. INTRODUCTION

As the quality of x-ray observations of elliptical galaxies has increased, the modest agreement with simple theoretical models has diverged. In bright ellipticals the x-ray emission is dominated by thermal radiation from optically thin interstellar gas. The radial variation of density and temperature in the hot gas, $\rho(r)$ and $T(r)$, can be determined from observations of the projected X-ray surface brightness and spectrum. But we show here that neither $\rho(r)$ nor $T(r)$ can be reproduced with gas dynamical calculations based on variations of the standard assumptions of galactic cooling flow theory.

In the usual theoretical approach the equations of gas dynamics are solved with source terms describing the rate that new gas flows into the interstellar gas, ejected by red giants in an old stellar population. The thermal energy of the interstellar gas is influenced by several effects: (i) the (kinetic) energy of newly injected gas that it inherits from the orbital motion of the parent stars, (ii) additional heating by Type Ia supernovae, and, most importantly, (iii) compressive heating in the galactic gravitational potential. The final gas temperature, $T \sim 10^7$ K, is comparable to the virial temperature of the galactic potential. Heating by supernovae cannot be too large otherwise the iron abundance in the hot interstellar gas would exceed observational limits or the heated gas would flow out of the galaxy as a wind, reducing the total x-ray luminosity L_x below the threshold of detectability.

Conversely, the interstellar gas cannot be free-falling rapidly in the galactic potential since the mass loss rate from evolving stars is insufficient to resupply the observed mass of interstellar gas in the freefall time for large ellipticals, $\lesssim 10^9$ yrs. For these reasons it follows that the hot interstellar gas is flowing very subsonically and the condition of hydrostatic equilibrium is satisfied to an excellent approximation at most galactic radii.

The main properties of gas in x-ray luminous ellipticals have been confirmed with evolutionary gas dynamical calculations, but many important details remain unexplained. Some inconsistencies between theory and observations have been known for some time. For example: the wide scatter in x-ray luminosity L_x for galaxies of similar optical luminosity L_B (Eskridge et al. 1995) and the often surprisingly low (and varied) mean iron abundance in the hot gas compared to that observed in the stars (Arimoto et al. 1997). It has also been recognized for many years that gas density slopes $d\rho/dr$ (derived from surface brightness observations) are less steep than those predicted by the most straightforward theoretical models. Recently, however, new inconsistencies have emerged. New observations of the gas temperature using ROSAT PSPC and ASCA (e.g. Davis and White 1996) indicate that the average gas temperature in massive ellipticals is $\sim 1.5-2$ times larger than the equivalent orbital temperature of the stars $T_* = (\mu m_p/k)\sigma_*^2$ where $\mu = 0.63$ is the mean molecular weight and m_p is the proton mass. The gas is much hotter than the stars. In addition gas temperature profiles $T(r)$ in most or all of the massive ellipticals studied so far show an increase by $30-40$ percent from the central values to about three effective radii where the temperature flattens or slowly decreases toward larger radii (Jones et al. 1997; David et al. 1994; Trinchieri et al. 1994; Mushotzky et al. 1994; Kim & Fabbiano 1995; Irwin & Sarazin 1996; Trinchieri et al. 1997). A plot showing these results can be found in Brighenti & Mathews (1997a). We show below that this peculiar temperature variation does not arise naturally in evolutionary flows based on gas lost from galactic stars. Finally, since all elliptical galaxies rotate at some significant level, their x-ray contours are expected to be significantly elongated perpendicular to the axis of rotation out to an effective radius or more (Brighenti & Mathews 1996; 1997b), yet most observed x-ray contours appear to be approximately circular!

In view of the serious nature of these observational inconsistencies with prevailing theory, in this paper we restrict our exploration of alternate theoretical models to spherical geometry. Our approach is to begin with a simple gas-dynamical model for the evolution of hot gas in a realistic galactic potential based on NGC 4472. We show that the final gas density and temperature variation in this model disagrees with observations of NGC 4472 in a variety of important ways. Then we vary the model parameters and assumptions to seek improvements, but instead only illustrate how insensitive the model is even to rather drastic alterations of the parameters. Finally, we show that the disagreement between the properties of interstellar gas in our gas dynamical model and those observed in NGC 4472 can be alleviated if large amounts of additional gas are supplied near the beginning of the galactic evolution. The same desirable result may be achieved by adding gas to the galaxy more slowly over many Gyrs, but we do not explore this possibility here. The important point is that elliptical galaxies can retain halos filled with very old hot gas. This gas may be a relic of an earlier time when these massive ellipticals were formed near the central focus of small groups. For some large ellipticals in Virgo this ancient gas has survived after the galaxy has entered the environment of this rich cluster.

2. NGC 4472 AND THE STANDARD ISM MODEL

Recently we have reviewed the x-ray observations of three bright nearby ellipticals: NGC 4472, 4636, and 4649. From the known gas density and temperature profiles in these galaxies and their optical properties, we determined the variation of total and stellar mass densities as functions of galactic radius assuming that the hot interstellar gas is in hydrostatic equilibrium (Brighenti & Mathews 1997a). For two of these galaxies, NGC 4472 and 4649, the hot interstellar gas is in equilibrium with the potential of the stars for $r \lesssim r_e$, the effective radius, but the potential of the massive dark halos dominates beyond r_e. For these two galaxies the agreement of the total mass and density with that of the stars alone over $0.1 \lesssim r/r_e \lesssim 1$ verifies that the mass to light ratio determined from the stars and the gas temperature determined from x-ray spectra are accurate and that hydrostatic equilibrium maintains. We can therefore be confident that the underlying mass structure of these galaxies is well

understood.

2.1. Properties of NGC 4472

For a realistic galactic model in which to test various gas dynamical models described below, we use the total mass $M_{tot}(r) = M_{dark}(r) + M_*(r)$ of NGC 4472 found by assuming hydrostatic equilibrium using gas temperatures and densities based on x-ray observations. The variation of gas density $n(r)$ for NGC 4472 plotted in Figure 1a combines results from ROSAT HRI and PSPC observations of Irwin & Sarazin (1996) and *Einstein* HRI observations of Trinchieri, Fabbiano & Canizares (1986). The analytic fit to the gas density $n(r) = \rho(r)/1.25m_p$ in Figure 1a is sum of functions $n(r) = \Sigma n_i(r)$ where $n_i(r) = n_o(i)[1 + [r/r_o(i)]^{p(i)}]^{-1}$. For 4472 we used three such functions with the following parameters: $n_o(i) = 0.095$, 0.00597, -.0004 cm^{-3}; $r_o(i) = 0.107$, 0.95, 10. in units of r_e; $p(i) = 2.0$, 1.14, 1.19. The gas temperature profile for NGC 4472 in Figure 1a is fit with a function of the form $T(r) = 2T_m[r_m/(r + r_{ot}) + (r/r_m)^q]^{-1}$ with parameters $T_m = 0.75 \times 10^7$ K, $r_m = 0.5r_e$, $r_{ot} = 0.75r_e$ and $q = 0$. Although the observed temperature is an average along the line of sight at projected radius R weighted by the local emissivity $\sim \rho^2$, we assume that the temperature at physical radius r is the same, i.e. $T(r) \approx T(R)$. This approximation is appropriate because of the steep decline of ρ with galactic radius (Brighenti & Mathews 1997a).

The total mass that confines the hot interstellar gas is found from the condition for hydrostatic equilibrium

$$M_{tot}(r) = -\frac{kT(r)r}{G\mu m_p}\left(\frac{d\log\rho}{d\log r} + \frac{d\log T}{d\log r}\right).$$

$M_{tot}(r)$ is plotted in Figure 1b. Also shown in Figure 1b is the de Vaucouleurs stellar mass distribution $M_*(r)$ determined from the optical data for NGC 4472: luminosity $L_B = 7.89 \times 10^{10} L_{B,\odot}$, distance $D = 17$ Mpc, effective radius $r_e = 8.57$ kpc, stellar mass to light ratio 9.20 (van der Marel 1991), and total stellar mass $M_{*t} = 7.26 \times 10^{11}$ $M_\odot$. M_{tot} and the local total density (Figure 1c) are dominated by the dark halo for $r \gtrsim r_e$ but within r_e the x-ray distribution is determined by the stellar potential alone. As noted earlier, the total mass in $0.1r_e \lesssim r \lesssim r_e$ is in excellent agreement with the expected stellar mass, $M_{tot} \approx M_*$. The galactic potential GM_{tot}/r that we adopt for our dynamic models for gas flow in NGC 4472 is based on $M_{tot}(r)$ shown in Figure 1b.

Iron abundance determinations for the hot gas in NGC 4472 vary with method and instrument used: $z_{Fe} = 0.20$ (Serlemitsos et al. 1993 with BBXRT), $z_{Fe} = 1-2$ (Forman et al. 1993 with ROSAT), $z_{Fe} = 0.63$ (Awaki et al. 1994 with ASCA), and $z_{Fe} = 1.18$ (Buote & Fabian 1997 with ASCA). Some, but not all, of this variation is due to significant differences in the adopted abundance for the sun or solar system (Ishimaru & Arimoto 1997). Arimoto et al. (1997) adopt a mean (emission-weighted) gas abundance $z_{Fe} = 0.33$ in solar units with $z_{Fe\odot} = 4.68 \times 10^{-5}$. In our models much of the interstellar iron comes from stellar mass loss. Gas ejected from stars at any radius is assumed to have the same iron abundance as the local parent stars. For the stellar iron abundance in NGC 4472 we assume a solar value at the galactic center which decreases as $z_{*Fe} \propto r^{-0.3}$ far from the galactic core (Arimoto et al. 1997), i.e. $z_{*Fe}(r) = 1.0/[1 + (r/r_b)^2]^{0.15}$ where $r_b = 200$ pc is the core or "break" radius of NGC 4472 (Faber et al. 1997). We have deliberately chosen a somewhat smaller central stellar iron abundance than the $z_{*Fe}(0) = 1.6$ adopted by Arimoto et al. (1997); previously it had been thought that z_{*Fe} followed the spectral features of Mg in the solar ratio, but it is now thought that Mg/Fe exceeds the solar ratio in bright ellipticals (Scott Trager, private communication). Since all of these parameters are highly uncertain, the absolute iron abundances we calculate are very approximate. Our main interest here are the relative emissivity-weighted abundances $\langle z_{Fe}/z_{Fe\odot}\rangle$ among the various dynamical models.

2.2. The Standard Model for the Hot Gas in NGC 4472: Model STD

The standard gas dynamics equations that describe the evolution of hot interstellar gas in ellipticals are:

$$\frac{\partial\rho}{\partial t} + \frac{1}{r^2}\frac{\partial}{\partial r}\left(r^2\rho u\right) = \alpha\rho_*,$$

$$\rho\left(\frac{\partial u}{\partial t} + u\frac{\partial u}{\partial r}\right) = -\frac{\partial P}{\partial r} - \rho\frac{GM_{tot}(r)}{r^2} - \alpha\rho_* u,$$

and

$$\rho\frac{d\varepsilon}{dt} = \frac{P}{\rho}\frac{d\rho}{dt} - \frac{\rho^2\Lambda(T)}{m_p^2} + \alpha\rho_*\left[\varepsilon_o - \varepsilon - \frac{P}{\rho} + \frac{u^2}{2}\right].$$

Here $\varepsilon = 3kT/2\mu m_p$ is the specific thermal energy. Both stars and supernova contribute mass to the interstellar gas, $\alpha = \alpha_* + \alpha_{sn}$, but the contribution

from supernovae α_{sn} is very small. An old stellar population expels gas at a rate $\alpha_*(t)\rho_*$ gm cm^{-3} s^{-1} where $\alpha_*(t) = \alpha_*(t_n)(t/t_n)^{-1.3}$, $t_n = 13$ Gyrs is the current time and $\alpha_*(t_n) = 5.4 \times 10^{-20}$ s^{-1} (Mathews 1989). The time variation of $\alpha_*(t)$ is surprisingly insensitive to the IMF assumed, but $\alpha_*(t_n)$ is only know to within a factor of ~ 2. As described above, $M_{tot}(r)$ is known directly from the observed gas temperature and density in NGC 4472 and the stellar density $\rho_*(r)$ is based on a de Vaucouleurs profile normalized to values appropriate to NGC 4472. The loss of thermal energy by optically thin thermal emission is described by the cooling coefficient $\Lambda(T)$ modeled after the results of Raymond, Cox & Smith (1976). The gas is assumed to be heated only by supernova of Type Ia since we assume that the early phase of galactic winds generated by Type II supernovae has already subsided at time $t = 1$ Gyr when we begin our calculations. The mean gas injection energy is $\varepsilon_o = 3kT_o/2\mu m_p$ where $T_o = (\alpha_* T_* + \alpha_{sn} T_{sn})/\alpha$. The local stellar temperature $T_*(r)$ is found by solving the equation of stellar hydrodynamics (with isotropic velocity ellipsoids) in the total mass potential of NGC 4472. Supernova heating of the interstellar gas is described by

$$\alpha_{sn} T_{sn} = 2.13 \times 10^{-8} \text{ SNu}(t) \ (E_{sn}/10^{51}\text{ergs})$$
$$h^{-1.7} \ (L_B/L_{B\odot})^{-0.35} \quad \text{K s}^{-1}$$

where $h \equiv H/100 = 0.75$ is the reduced Hubble constant and we adopt $E_{sn} = 10^{51}$ ergs as the typical energy released in a supernova event. This equation incorporates the mean stellar mass to light ratio for elliptical galaxies from van der Marel (1991), $M_{*t}/L_B = 2.98 \times 10^{-3}(L_B/L_{B\odot})^{0.35} h^{1.7}$. (The individually determined mass to light ratio for NGC 4472, $M_{*t}/L_B = 9.20$, is slightly lower than that of the average elliptical having the same L_B.) For our galaxy model (based on NGC 4472) we take $L_B = 7.89 \times 10^{10} L_{B\odot}$. Although there is some information available about the current Type Ia supernova rate in ellipticals (Turatto, Cappellaro & Benetti 1994), almost nothing is known about supernova rates in the distant past. For this paper we adopt a power law to describe a varying rate of Type Ia supernovae:

$$\text{SNu}(t) = \text{SNu}(t_n)(t/t_n)^{-p}$$

with $p = 1$ and $\text{SNu}(t_n) = 0.04$ SNu (1 SNu = 1 supernova every 100 years in stars having luminosity $L_B = 10^{10} L_{B\odot}$). We assume each supernova ejects 1.4 $M_\odot$ into the local interstellar gas and that half of this, 0.7 $M_\odot$, is iron. The iron abundance currently observed in the hot gas provides a global constraint on the past supernova rate and our parameters are chosen with this constraint in mind. Finally, the de Vaucouleurs model for the stellar component in our model galaxy extends out to radius $r_t = 100$ kpc where the stellar density is very low, but the dark halo continues out to 470 kpc where its total mass is $M_{dark,t} = 2.7 \times 10^{13} M_\odot$. Since the gas is ejected from stars within 100 kpc, the much more extensive dark halo – which may resemble those of central ellipticals in groups – is irrelevant to most of the following gas dynamical solutions.

The gas-dynamical equations are solved using a standard one-dimensional second order Eulerian code. We use reflection boundary conditions at the origin and outflow boundary conditions at the outer boundary, $r = 470$ kpc.

2.3. Comparison of Standard Model (STD) and Observations

Along with the observations of NGC 4472 in Figure 2 we also show the current variation of density and temperature predicted by solving the gas dynamical equations above. These equations are solved beginning with no gas in the galaxy at $t = 1$ Gyr and carried forward to the current time, $t_n = 13$ Gyr. This gas-free initial condition can be understood if SNII explosions had driven strong winds out of the galaxy at early times (Mathews 1989; avid et al. 1991; Loewenstein & Mushotzky 1996). The elliptical in our gas dynamical model is assumed to be isolated so that gas can flow out beyond the galaxy if it wishes.

The deficiencies of the model are apparent! The predicted density gradient for this "standard model" (STD) shown in Figure 2 is steeper than the observed density distribution throughout the entire galaxy. Traditionally this discrepancy has been recognized only in the central regions. The projected x-ray surface brightness of the model galaxy $\Sigma_x(R)$ is also steeper than that observed for NGC 4472. This density discrepancy still persists for models, not shown in Figure 2, in which the calculation is begun at $t = 0.1$ Gyr to increase (by ~ 3) the total amount of gas ejected from the stars. Although the gas temperature predicted by our model is roughly comparable with observed values shown in Figure 2, it is definitely too low at all radii by a factor of $\sim 2 - 3$ except perhaps within a few kpc from the center.

In addition, the shape of our computed temperature variation $T(r)$ does not have the characteristic positive gradient dT/dr out to $r \sim 3r_e$ that is typical of most or all galactic cooling flows observed so far (Brighenti & Mathews 1997a). For deep gravitational potentials, as for example where the de Vaucouleurs mass dominates, the temperature gradients determined by our gas dynamical model are slightly negative at most radii. This negative gradient is due to the work done by gravitational compression; as gas expelled from stars at radius r loses energy by radiation, it sinks deeper in the galactic potential. For shallower potentials, however, dT/dr can be positive, but such potentials are not realistic models for galaxies like NGC 4472. We have not illustrated the velocity field corresponding to the model in Figure 2 since it is not directly observed. The flow velocity is negative throughout most of the galaxy but becomes slightly positive in the very tenuous gas at $r \gtrsim 160$ kpc. Within this radius the velocity gradually increases inward reaching -20, -50, and -140 km s^{-1} at 10, 1, and 0.32 kpc respectively.

The mean interstellar iron abundance in model STD, weighted by $\rho^2\Lambda$, is $\langle z_{Fe} \rangle = 1.03$ in solar units which is higher than the mean (mass-weighted) stellar value $z_{*Fe} \approx 0.34$. If the observed interstellar abundance in NGC 4472 is as low as Arimoto et al. (1997) claim, $z_{Fe} \approx 0.33$, then our (rather low) current supernova rate $\mathrm{SNu}(t_n) = 0.04$ may still be an overestimate.

In model STD essentially all of the gas lost from the stars is retained within the galaxy. Most of the gas created in model STD from $t = 1$ to 13 Gyr, about 7.2×10^{10} $M_\odot$, eventually cools at the very center of the flow leaving only a relatively small mass of hot gas, 0.6×10^{10} $M_\odot$, to produce the x-ray luminosity L_x. In more realistic rotating cooling flows the gas cools to a disk (Brighenti & Mathews 1996; 1997b). In Table 1 we list several global parameters of the standard model STD and its variants described below.

3. VARIATIONS ON THE STANDARD MODEL

3.1. Mass Dropout: Model DO

The conventional theoretical means of flattening steep density profiles in galactic cooling flow models is straightforward: remove hot gas from the cooling flow near the galactic center! In addition to correcting the density profile, this much-used assumption of "mass dropout" was also motivated by the possibility that thermal instabilities could develop from hypothetical inhomogeneities in the cooling flow gas (Fabian & Nulsen 1977; Stewart et al. 1984; White & Sarazin 1987a, 1987b, 1988; Thomas et al. 1987; Vedder, Trester & Canizares 1988; Sarazin & Ashe 1989; Bertin & Toniazzo 1995). However, such thermal instabilities do not grow in the expected manner. Low amplitude thermal instabilities are generally stable (Balbus 1991) and coherent non-linear perturbations of larger amplitude oscillate radially in the cooling flow atmosphere (Loewenstein 1989) so that they are alternatively overdense and underdense relative to ambient gas, reducing or eliminating the growth rate of the instability. Even if instability were possible, such initially overdense, oscillating regions are not likely to remain coherent since hydrodynamical models show conclusively that they disintegrate by Rayleigh-Taylor and Kelvin-Helmholtz instabilities before completing a single oscillation (Hattori & Habe 1990; Malagoli et al. 1990). Moreover, the origin of the required inhomogeneities is also unclear since there is no known source of entropy perturbations on the appropriate scales in the interstellar gas (Mathews 1990).

Nevertheless, the problem of steep theoretical density profiles is clearly still present in Figure 2! In view of this and in deference to those many astronomers who have invoked mass dropout, we now describe some models for NGC 4472 using the standard dropout assumptions which are expected to flatten $d\rho/dr$. When dropout is included, an additional term $-q\dot{\rho}/t_{do}$ is introduced on the right hand side of the equation of continuity but the equations of motion and thermal energy remain unchanged. The characteristic dropout time is usually assumed to be the time for local radiative cooling, $t_{do} = 5m_pkT/2\mu\rho\Lambda$ (e. g. Sarazin & Ashe 1989), and the constant dimensionless parameter q controls the amount of mass dropout. Gas is removed from the flow on the spot, i.e. t_{do} is assumed to be much less than the local flow time. Although $t_{do} \ll t_{flow} \approx r/|u|$ is widely used in mass dropout calculations, it is often strongly violated. The rate that gas is removed from the flow is proportional to $\rho t_{do}^{-1} \propto \rho^2$ and therefore increases closer to the galactic center as required to flatten $d\rho/dr$. The temperature of the *remaining* gas that does not participate in the dropout is increased. This occurs since after dropout less gas is present at small radii to support the weight of the same large global mass of interstellar gas so compressional heating is in-

tensified at small radii to maintain hydrostatic pressure equilibrium. However, as gas cools and undergoes local dropout it will emit radiation from systematically cooler gas. The net temperature observed at any radius is therefore a weighted mean between the background flow and the gas that is dropping out. The local x-ray emissivity $\epsilon_{\Delta E}$ into the ROSAT band ($\Delta E = 0.2 - 2.4$ keV) is increased by a factor $(1+q\Delta_0)$ and the local mean temperature is lowered from T to $T_{eff} = T(1+q\Delta_1)/(1+q\Delta_0)$ where T is the temperature of the gas that has not yet dropped out and Δ_0 and Δ_1 are defined by

$$\Delta_n = \frac{1}{T^{1+n}} \frac{\Lambda}{\Lambda_{\Delta E}} \int_0^T (T')^n \frac{\Lambda_{\Delta E}}{\Lambda} dT'.$$

The functions $\Delta_0(T)$ and $\Delta_1(T)$ are plotted in Figure 3.

Figure 4 shows the density and temperature structure of a cooling flow with mass dropout using $q = 1.2$. A comparison with Figure 2 reveals that $d\rho/dr$ is indeed flattened within about 40 kpc by the dropout but the flow at larger radii, where the dropout is very small, is unchanged. The slope $d\rho/dr$ between 1 and 10 kpc is almost flattened to the slope of the NGC 4472 density profile and a further increase in q would bring the slope there into agreement. However, dropout has also *lowered* the gas density in the bright inner galaxy so $\alpha_*(t_n)$ would need to be increased by $\gtrsim 4$ to bring the dropout solution into approximate agreement with local NGC 4472 densities within 10 kpc. Such a large increase in $\alpha_*(t_n)$ may be inconsistent with reasonable stellar IMF slopes and mass cutoffs (Mathews 1989). In any case, the gas density is very much lower than observed values at $r \sim 100$ kpc where the x-ray observations are still very reliable. Although the beneficial influence of dropout on the density profile near the core has long been recognized, its failure to flatten $d\rho/dr$ at larger radii has been unappreciated probably because most previous dropout solutions also used the steady state approximation which is known to diverge and become unreliable at large galactic radii (e.g. Vedder, Trester & Canizares 1988).

But the most serious problem for the cooling flow with dropout is seen in the temperature profile in Figure 4. The light solid line shows the temperature variation of the background gas which is increased over that in Figure 2 as explained above. When the cooler temperatures of locally dropping out gas is included, however, the apparent gas temperature $T_{eff}(r)$ (heaver solid line in Figure 4) is slightly *lower* than the temperature without dropout shown in Figure 2. According to the usual dropout assumptions, the dropout causes a lowering of the gas temperature even at very large galactic radii (Figure 4) since the small mass that drops out there is compensated by the much longer dropout time t_{do}. Therefore, even if mass dropout were a physically acceptable process, it fails to correct the deficiency of gas at large galactic radii (large negative $d\rho/dr$) and moves the computed gas temperatures further from observed values.

Aside from the many theoretical arguments against the widely-used assumption of mass dropout, x-ray observations also indicate that galactic cooling flows cannot have a pronounced global multiphase character in which regions of low entropy are cooling out. Unless there is a conspiracy of compensating effects, the near perfect agreement of the total and stellar mass in Figure 1b – and also for NGC 4649 (Brighenti & Mathews 1997a) – are inconsistent with mass dropout. In the presence of dropout the apparent temperature is lowered from T to T_{eff} which reduces $M_{tot}(r)$ determined from the equation of hydrostatic equilibrium. Also the density gradient is flatter, as in Figure 4, implying a smaller confining total mass than actually exists. But the density shown in Figure 4 represents that of the background flow and has not been corrected for emission from regions of higher density that are dropping out; so the reduction in $M_{tot}(r)$ is not as large as would appear from Figure 4. If mass dropout is really present and not allowed for in determining $M_{tot}(r)$ from the equation of hydrostatic equilibrium, Gunn & Thomas (1996) have shown that the apparent total confining mass is lowered by 20 to 60 percent. In typical dropout models, gas is removed from the flow instantaneously. But the pressure gradient in the flow readjusts only after a local sound crossing time, too slow to follow the effects of dropout on the gas density and temperature. However, the total mass (Figure 1b) determined from observed gas $\rho(r)$ and $T(r)$ (Figure 1a) agrees to within 10 percent of the independently determined stellar mass for $0.1r_e \lesssim r \lesssim r_e$. This is strong observational evidence that distributed mass dropout is not dominating the cooling flows observed in these two well-observed ellipticals.

3.2. Non-uniform α_*: Model NUA

Since mass dropout has failed to account for the observed interstellar gas in NGC 4472, we abandon

caution and explore models in which the fundamental coefficients in the source terms of the gas dynamical equations are varied in an arbitrary fashion. For example, suppose proportionally more gas is ejected from stars further from the galactic core, then it might be expected that the ISM density profile would flatten. In an attempt to investigate this possibility, we impose an arbitrary spatial dependence on the stellar mass loss coefficient in which the stellar mass loss is enhanced at larger radii: $\alpha_* = \alpha_*(t_n)\ (r/r_a)^a\ (t/t_n)^{-1.3}$. We have considered various values of $a > 0$ and r_a. A representative example of the resulting flow at t_n with $a = 0.4$ and $r_a = r_e$ is shown in Figure 5. Even though more (less) gas is being expelled from the stars at large (small) radii, the final solution for both $n(r)$ and $T(r)$ is almost identical to that in Figure 2 with uniform α_*! The overall vertical normalization has changed slightly since the total mass lost from the stars $M_{*t} \int \alpha_* dt$ is somewhat different, but the slope of the final density profile is very insensitive to the radial dependence of the stellar mass loss rate for all of the a-r_a pairs we have considered. Evidently this result is due to the insensitivity of the gas temperature profile to α_* and the necessity for the gas to adjust to just that radial density distribution that achieves hydrostatic equilibrium.

3.3. Non-uniform Λ: Model NUL

Since none of the previous modified solutions has increased the gas temperature toward observed values, particularly further out in the galaxy, perhaps an adjustment of the radiative cooling rate can accomplish this. Although the total radiative cooling coefficient $\Lambda(T)$ changes slowly with temperature, $\Lambda(T = 10^6) \approx 3\Lambda(T = 10^7)$, an additional dependence on metallicity should also be present at some level and this has not been considered in the models previously discussed. Since the metallicity z of the hot cooling flow gas increases inwards and $d\Lambda/dz > 0$, we consider the evolution of cooling flows with arbitrarily enhanced cooling at small radii: $\Lambda(T, r) = (r/r_s)^s\ \Lambda(T)$ where $s < 0$ and $\Lambda(T)$ is the cooling rate used in the standard solution (Figure 2). We have solved the cooling flow hydrodynamics with several s-r_s pairs (keeping all other parameters identical to those of the standard model) and the results for $s = -0.6$ and $r_s = 3r_e$ are shown in Figure 6 at time $t_n = 13$ Gyr.

As a result of this rather large adjustment in Λ the central gas temperature has increased slightly at $r \lesssim 3r_e \approx 26$ kpc, but the gas temperature is still much lower than that observed in NGC 4472. However, at $r \gtrsim 3r_e$ the computed temperature $T(r)$ is almost unchanged from that of the standard model in Figure 2. The slope of the density profile dn/dr in Figure 6 is significantly improved within about 10 kpc, but is still much too small further out. Our results for other s-r_s pairs are similar so we must conclude that drastic, unphysical adjustments to the radiative cooling rate cannot bring the model temperatures (or densities) into satisfactory agreement with observations.

3.4. Higher Supernova Rate: Models SN1 and SN2

We now explore the possibility of raising the gas temperature by increasing the supernova rate above that used in the standard solution of Figure 2. If the gas can be heated in this manner its pressure and density scale heights will also increase, flattening dn/dr and improving solutions for both $T(r)$ and $n(r)$. Of course as the supernova rate SNu(t) is increased, we can anticipate that the iron abundance in the hot gas will also increase even further beyond the observed mean value in the hot gas (Loewenstein & Mathews 1991). But we shall avert our concern about the iron abundance for the time being, hoping that a separate solution for reconciling the iron abundance can be found later by some exotic theoretical artifice.

The supernova rate $\mathrm{SNu}(t) = \mathrm{SNu}(t_n)(t/t_n)^{-p}$ (where $p > 0$) can be altered either by raising p to increase the past rate of Type Ia supernovae or by increasing the coefficient SNu(t_n) which increases SNu at all times. Our value $p = 1$ for the standard solution allows for some reasonable cosmic evolution but is less than the exponent 1.3 in the stellar mass loss rate $\alpha_* \propto t^{-1.3}$. Ciotti et al. (1991) have shown that galactic winds can occur during the early evolution if $p > 1.3$ and propose that the dynamically unsteady transition from winds to cooling flows at the current time may account for the strong spread observed in L_x/L_B. However, the standard solution in Figure 2 indicates a deficiency of interstellar gas which would be further reduced by galactic winds. Therefore, we explore here the heating effects on the interstellar gas using larger SNu(t_n) which increases the supernova rate equally at all times while maintaing a cooling flow throughout the galactic evolution.

The solid lines in Figure 7 show the status of the hot interstellar gas in our model SN1 for NGC 4472 using $\mathrm{SNu}(t_n) = 0.25$, about six times larger than

the standard model in Figure 2. The gas temperature throughout the galaxy has in fact been increased, but only by about 20 percent, far less than the factor that SNu(t_n) is increased. The gas density profile in Figure 7 is also significantly improved, but is still steeper than the observed slope. As expected, the mean iron abundance in the interstellar gas $\langle z_{Fe} \rangle \approx 4.41$ (Table 1) far exceeds any of the values observed in NGC 4472 and by a much larger factor than the standard model STD.

Although increasing the supernova rate has a beneficial influence on both $n(r)$ and $T(r)$, SNu(t_n) cannot be raised further without driving a galactic wind. Already when SNu(t_n) = 0.3 much of the interstellar medium is moving outwards at time $t_n = 13$ Gyrs and the gas density has declined substantially throughout the galaxy. The dashed contours in Figure 7 show the density and temperature structure at t_n for the wind solution SN2 that develops when SNu(t_n) = 0.45. The density has dropped to unacceptably low values and the temperature far exceeds observed values.

4. MODELS WITH ADDITIONAL CIRCUMGALACTIC GAS: MODELS EXG1 AND EXG2

Having considered a variety of both modest and radical perturbations of our initial standard model for NGC 4472, all the same problems still remain: the slope of the density is too steep, the mass of hot gas at large galactic radii is too small, the temperature is too low by about a factor of 2, and the shape of the temperature profile is wrong.

A clue to the resolution of this problem may lie in the total amount of hot gas observed in NGC 4472 (Trinchieri, Fabbiano, & Canizares 1986; Irwin & Sarazin 1996; Brighenti & Mathews 1997a). At $r =$ 140 kpc, the largest galactic radius at which reliable gas density measurements are available for NGC 4472, the total mass in hot gas is about $M_{gas} = 3.5 \times 10^{10}$ $M_\odot$, about 7 percent of the total stellar mass of the galaxy. Using our standard mass loss rate $\alpha_*(t)$ we expect that approximately 8.5 percent of the total stellar mass of the galaxy should have been ejected into the interstellar medium from 1 to 13 Gyrs. However, allowance must be made for the large fraction of this gas that cools. The mass budget of our standard model in Table 1 indicates that about 92 percent of the gas ejected by stars over this cosmic time interval has already cooled and is no longer available to emit x-rays. Therefore, by analogy with the standard solution, the amount of gas observed in NGC 4472 out to 140 kpc implies a minimum initial total gas mass of at least 6.3×10^{11} $M_\odot$ – this is about 10 times larger than the mass that can be ejected by galactic stars! We conclude that *most of the mass that contributes to cooling flows in galaxies like NGC 4472 has not come from mass lost by galactic stars since time 1 Gyr.*

When extra gas is introduced into the models many new and uncertain parameters must be determined. Is most of the extra gas present at early times or is it slowly added during the Hubble time? What is the origin of this extra gas: is it primordial or has it been enriched and ejected by galactic winds from the massive elliptical or other nearby galaxies? What is the temperature and density (entropy) of this extra gas? Since the additional gas must be about twice as hot as that in the standard solution, what total mass of dark matter is required to bind the additional gas? Although we have explored some of these questions, we shall not attempt to answer them in detail here. Our more limited objective here is to present results of some approximate and preliminary calculations that nevertheless conclusively illustrate the many benefits of additional hot gas in understanding the nature of cooling flows in bright elliptical galaxies.

Our provisional astrophysical interpretation of the source of the extra gas required, as discussed below, is that all bright ellipticals with $T_{gas} \sim 1.5 - 2T_*$ (Davis & White 1996) were originally formed in small galaxy groups of the sort discussed by Mulchaey et al. (1996). These authors have shown that a significant fraction of small groups of galaxies contain dominant bright ellipticals and that most or all of the observed diffuse, x-ray emitting gas in these groups is usually closely associated with the central massive elliptical. This implies that the source of the hot gas is closely related to the creation of bright elliptical galaxies, probably by mergers and tidal mass transfers. Dynamical studies of the evolution of galaxies in elliptical-forming groups (Merritt 1985; Bode et al. 1994; Garciagomez et al. 1996; Athanassoula et al. 1997; Dubinski 1997) require that ellipticals were formed early in the dynamical evolution of groups when mergers and tidal interactions were most likely; if so, both the elliptical galaxy and the hot interstellar gas surrounding it are very old. With this in mind, we consider models in which the extra hot gas is already present at the time $t = 1$ Gyr when our model calculations begin. We shall not discuss here the alternative

possibility that gas gradually flows into large elliptical galaxies over the Hubble time.

To construct a variant of our standard model having large amounts of hot gas at $t = 1$ Gyr, we consider a (somewhat arbitrary) gas density distribution at this early time described by $n(r) = n_o[1+(r/r_c)^2]^{-3/4}$ where $n_o = 0.5$ cm^{-3} and $r_c = 0.20$ kpc, out to radius $r = 62$ kpc. At $r > 62$ kpc we assume $n(r) = 10^{-4}$ cm^{-3} out to $r = 470$ kpc where the gas is abruptly terminated. The initial gas temperature $T = 1.2 \times 10^7$ K and iron abundance $z_{Fe} = 0.1$ are uniform in this extended gaseous halo. We consider two models beginning with this extra gas: in the first (EXG1) α_* has the standard value and time dependence; in the second (EXG2) α_* is reduced by half at all times. All other parameters are those of our standard solution.

As in the previous calculations, we assume that the dark halo of our model for NGC 4472 extends out to 470 kpc where stars and dark halo have a combined total mass of 27×10^{12} $M_\odot$. This is large, but comparable with the masses of small groups of galaxies found by Mulchaey et al. (1996). The total initial mass of hot gas is $M_{hot} = 1.50 \times 10^{12}$ $M_\odot$ within 470 kpc, but only $M_{hot} = 0.019 \times 10^{12}$ $M_\odot$ of this gas is within 100 kpc which includes the stellar part of the galaxy. Since the total stellar mass is 0.72×10^{12} $M_\odot$, the initial ratio of total baryonic to dark matter is 0.08, acceptably close to the expected cosmological value. It is clear from simple dynamical considerations that the dark matter halo must extend out considerably beyond ROSAT observations at 140 kpc since if the gas and dark matter were truncated at this radius a rarefaction wave would move into the galaxy in $\lesssim 1$ Gyr and sharply reduce gas densities and temperatures at $r \lesssim 140$ kpc. Therefore our assumptions about the mass of initial gas and dark matter are consistent with current observations of NGC 4472.

In Figure 8 we show temperature and density profiles in the hot interstellar gas at $t_n = 13$ Gyrs for two models having the initial gas configuration described above. The first model (EXG1), shown with dashed lines, is computed with other parameters identical to the standard model. The gas density is in excellent agreement with the observations for radii $r \gtrsim 6$ kpc $= 0.7r_e$ but steepens further in. In the second model (EXG2) α_* is reduced by a factor of 2 so that the galactic stars contribute less to the density profile within r_e. This model shown with solid contours in Figure 8 is an even better fit to the overall observed density profile and its luminosity, $L_x = 49 \times 10^{40}$ ergs s^{-1}, is very close to that observed for NGC 4472, $L_x = 45.6 \times 10^{40}$ ergs s^{-1} (Eskridge, Fabbiano, & Kim 1995) when scaled to $d = 17$ Mpc. For either model, the gas density near the outermost observed radius (~ 140 kpc) is in excellent agreement with observations. The temperature profile for either model is also in adequate agreement with observations. This consistency with current observations of NGC 4472 follows from the extended region of (constant density) hot gas beyond 62 kpc that we assume at time $t = 1$ Gyr; if only this component of the initial hot gas is retained, the agreement of the model at $t = 13$ Gyrs with observed $n(r)$ and $T(r)$ is about the same as that shown in Figure 8. Our objective here is not to cosmetically adjust the parameters of the initial gas distribution by trial and error until the agreement with the present day $n(r)$ and $T(r)$ is perfect. Instead our less ambitious objectives are (i) to demonstrate that very hot gas can be retained by massive ellipticals throughout the Hubble time and (ii) that this gas is the key to understanding present-day observations. In a more comprehensive model, the detailed properties of the initial (or subsequently added) gas must be a natural consequence of more global cosmological considerations.

5. ASTRONOMICAL IMPLICATIONS OF CIRCUMGALACTIC GAS

We conclude that gas ejected from stars evolving since the epoch of strong galactic winds, ~ 1 Gyr, is insufficient to account for the density and thermal structure observed in elliptical cooling flows. This conclusion is not unique to NGC 4472. Davis & White (1996) have shown that ROSAT temperatures for bright ellipticals are systematically higher than mean stellar temperature by $\sim 1.5 - 2$. Brighenti & Mathews (1997a) have noticed that the normalized radial variation of gas temperature $T(r/r_e)$ for six bright ellipticals having good ROSAT and ASCA temperatures is remarkably similar, regardless of the environmental context of the galaxy. Some of these galaxies are dominant ellipticals in small groups or poor clusters (NGC 5044: David et al. 1994; NGC 507: Kim & Fabbiano 1995; NGC 1399: Jones et al. 1997) while others are associated with the Virgo cluster (NGC 4636: Trinchieri et al. 1994; NGC 4472: Irwin & Sarazin 1996; NGC 4649: Trinchieri et al. 1997). Because of the apparently universal thermal structure among these galaxies, we conjecture that all these bright ellipticals originally formed

as the primary galaxy in a small group. The uniformity in the currently observed temperature profiles implies that the initial evolution of these ellipticals must have been very similar. With time some of these luminous ellipticals have now entered larger clusters where they have retained much of the gas inherited from the group environment. Certainly NGC 4472 is consistent with this interpretation since it is the central galaxy in a Virgo sub-cluster. Although all three Virgo galaxies (NGC 4636, 4472, and 4649) have the same positive temperature gradient at $r \lesssim 3r_e$, NGC 4649 has noticeably less hot interstellar gas than 4472 and 4636. This may be explained by the apparent proximity of NGC 4649 to the center of the Virgo cluster: hot interstellar gas at large galactic radius that initially contributed to the production of $dT/dr > 0$ in the central regions of NGC 4649 has since been ablated away by the velocity of 4649 relative to the intercluster medium. The pressure of the initial outer gaseous halo in 4649 has now been replaced by that of the diffuse hot gas in Virgo. Alternatively, NGC 4649 could have been originally a subordinate member of a small group of galaxies when its outer halo was tidally transferred to the group-dominant elliptical. These considerations are only appropriate for massive ellipticals for which current observational data for $\rho(r)$ and $T(r)$ are available. The radial interstellar structure in less luminous ellipticals may differ: they may have less hot gas, lower overall temperatures and and steeper density gradients, resembling our standard model in Figure 2. Perhaps AXAF can answer this question in more detail.

How is the characteristic temperature profile $T(r)$ in massive galaxies produced? For further insight into this, we calculated the gas dynamical flow for model EXG1:0, a variant of model EXG1 with no gas contribution from stellar mass loss or supernovae. After 13 Gyrs the temperature of model EXG1:0 is in excellent agreement with observed temperatures of NGC 4472 within about 8 kpc from the galactic center (see Figure 8). At larger radii, however, the gas is much hotter, rising to a maximum 2×10^7 K at 35 kpc then dropping to 1.5×10^7 K at 80 kpc. At all galactic radii shown in Figure 8, the temperature of externally provided gas in our model with no stellar gas $T(EXG1:0)$ is much higher than $T(STD)$, the gas temperature resulting from stellar mass loss alone (Figures 2 and 8). Evidently, the reasonably successful temperature agreement of model EXG1 with NGC 4472 observations is due in part to the mixing of hot circumgalactic gas with relatively cooler gas ejected from the stars. At any radius $r \lesssim 100$ kpc (which includes all of the stellar system), $T(EXG1)$ is an approximate thermal average of $T(STD)$ and $T(EXG1:0)$, weighted by the relative masses contributed at each radius by stellar mass loss and inflow of circumgalactic gas. By tagging the external gas and that from the stars with different abundances, we have determined (at time $t = 13$ Gyrs) for model EXG1 that about 60-70 percent of the gas at $r \lesssim r_e = 8.57$ kpc comes from the stars while at $r \approx 75$ kpc the stellar contribution has dropped to 10 percent. This fractional contribution is consistent with the relative temperatures of the three models shown in Figure 8 where it is seen that $T(EXG1:0) > T(EXG1) > T(STD)$ at all radii, although $T(EXG1:0)$ is closer to $T(EXG1)$ at large radii and closer to $T(STD)$ at $r \lesssim r_e$. We recognize that this argument is only approximate because the flow structure $u(r)$ in these three models is different. Nevertheless, it is clear that the characteristic temperature profile $T(r)$ observed in many bright ellipticals including NGC 4472 – rising from $T \sim T_*$ near the origin to 1.5 - 2 T_* at $r \sim 3r_e$ then becoming approximately isothermal – is a signature of the thermal combination of two sources of hot interstellar gas.

Where does the circumgalactic gas come from and why is it so hot? At present we cannot be entirely certain about the origin of this gas, but it is likely that its original source was "secondary infall" or the reversal of the Hubble flow surrounding positive density fluctuations that grow to become massive ellipticals or small groups. Upon arrival at the young galaxy, the infalling gas passes through a strong shock that raises its temperature to approximately the local virial temperature $T_{vir} \approx (\mu m_p/2k)GM_{tot}/r$ in the halo (Bertschinger 1985). It is likely that Type II supernovae from massive stars further heated and enriched the interstellar gas during the early stages of galactic formation. In the mass distribution for NGC 4472 (Figure 1b) T_{vir} increases by a factor 2.1 from $r = r_e$ to $r = 10r_e$; this may explain why the circumgalactic gas located at $r \gg r_e$ is hotter than the stars as required in our successful models and indicated by the observations of Davis & White (1996). Subsequently, the hot halo gas and dark matter may have been dynamically transferred between galaxies while they were members of small groups.

The introduction of rather large masses of hot gas

into ellipticals at early times may either resolve or complicate other problems that have received much attention over the years. For example, the wide scatter in L_x for given optical luminosity L_B may result from tidal exchanges of this extended halo gas component between ellipticals having similar L_B within the small groups in which they were formed (Mathews & Brighenti 1997). The general circularity of x-ray isophotes in rotating, massive ellipticals must also be understood in the context of circumgalactic gas. Brighenti & Mathews (1996) have shown that even the modest rotation of the stellar component observed in massive ellipticals is sufficient to produce strongly rotating disk configurations in the hot interstellar gas, assuming that the interstellar gas derives only from stellar mass loss. The x-ray images are flattened perpendicular to the axis of rotation. However, if the gas expelled from stars is overwhelmed by inflowing low angular momentum hot gas from the outer galaxy, the x-ray isophotes will appear more circular. But it is unclear if the circumgalactic gas would be expected to have less rotation. [Flattened x-ray isophotes may nevertheless still be present in rapidly rotating ellipticals of moderate or low luminosity (Brighenti & Mathews 1997b)]. The presence of additional gas in bright ellipticals both complicates and clarifies the interpretation of the iron abundance observed in the hot gas. Even when no circumgalactic gas is present, gas dynamical cooling flow models predict that the interstellar iron abundance should be less than that in the stars, provided the Type Ia supernova rate is very low; this occurs because the hot gas flows inward through a stellar system having a negative radial abundance gradient. But the disparity between high stellar and low gas abundances is so large that some have questioned the validity of abundance determinations from x-ray spectra (Arimoto et al. 1997; Renzini 1997). The Type Ia supernova rate in our standard model STD is comparable with the low rate observed, but still may produce too much iron. Nevertheless, we expect that observed iron abundances represent a combination of iron from stellar ejecta and circumstellar gas – of unknown abundance – that flows in from large galactic radii. The iron abundance in our model EXG2 is in fact lower than that of the standard model (Table 1), but not by very much for the parameters we considered. However, Loewenstein (1996) has pointed out that ellipticals having the largest amount of extended, circumgalactic gas have on average *higher* iron abundances, contrary to the expected trend.

6. CONCLUSIONS

We have attempted without success to derive the known density and temperature structure in NGC 4472 using the usual equations of gas dynamics and standard cooling flow assumptions. Our mass model for NGC 4472, based on hydrostatic equilibrium, is fully self-consistent and is not likely to be incorrect. In our attempts to bring the results of dynamical models into agreement with observations of NGC 4472, we considered mass dropout, spatially variable stellar mass loss and radiative emission rates, and higher supernova rates. Invariably, the total amount of hot gas generated by stellar mass loss that remains at the present time is insufficient, particularly at large galactic radii, and the density slope is too steep. The steepness of $d\rho/dr$ is obviously correlated with the relatively low gas temperatures $T \approx T_*$ that result from thermalization of stellar mass loss and supernova rates limited by the known iron abundance in the interstellar gas.

All these difficulties are resolved when additional hot gas is provided from the outer regions of the galactic potential. We are not the first to consider additional gas flowing into galactic cooling flows. Within the context of steady state solutions, both Thomas (1986) and Bertin & Toniazzo (1995) discussed the advantages of inflowing gas at the outer parts of the galaxy and both studies constrained their theoretical results to match observed properties of NGC 4472. The need for large gas masses in addition to that provided by stellar mass loss is already evident from the high gas mass indicated by ROSAT observations of NGC 4472 and other similar bright ellipticals. The gas density in NGC 4472 at $\sim$ 140 kpc, the outer limit of reliable x-ray surface brightness observations, is unstable to rapid outflow unless both the gas and the dark halo extend to significantly larger radii. We have therefore considered an initial configuration for NGC 4472 in which most of the original baryonic matter is in an extended hot gas phase and have shown that much of this gas can be retained over the Hubble time. Our model for the initial gas configuration is by no means unique, but serves to demonstrate the possible retention of very old hot gas in massive ellipticals.

The total mass of initial hot gas we consider within the large galactic halo (of radius r = 470 kpc) at

$t = 1$ Gyr, $M_{hot} = 1.50 \times 10^{12}\ M_\odot$, is about 2.1 times larger than the stellar mass. The temperature is initially uniform and hot, $T = 1.2 \times 10^7$ K. This gas and the dark galactic halo are assumed to extend out to $r = 470$ kpc. After following the gas dynamical evolution, by time $t_n = 13$ Gyr the mass of hot gas within $r = 470$ kpc is reduced by cooling and outflow to $0.40 \times 10^{12}\ M_\odot$. The mass of hot and cooled gas within the central, stellar part of the galaxy, $r \lesssim 100$ kpc, $M_{hot} = 0.04 \times 10^{12}\ M_\odot$ and $M_{cold} = 0.03 \times 10^{12}$ $M_\odot$, are both very much less than the total stellar mass, $M_{*t} = 0.72 \times 10^{12}\ M_\odot$. If the cooled gas formed into relatively low mass stars, the stellar mass to light ratio would not be affected. As gas from the reservoir of hot gas in the outer galaxy flows inward toward the stellar component, its temperature remains high, similar to values observed, $T \sim 1.5 - 2T_*$ and positive temperature gradients are generated within a few r_e, just like the observed pattern. Although both gas and stars reside in the same potential, the stars are confined to just the central regions and therefore have a mean temperature that is less than the more extensive gas. Since the gas is hotter, the gas density profile is flattened at all radii in conformity with observation.

The addition of hot gas to the outer regions of elliptical galaxies, either initially or over time, does not account only for the observations of NGC 4472, but is essential to understand similar model deficiencies in all massive ellipticals. Moreover, the similarity in observed $T(r)$ in most or all bright ellipticals observed so far (Brighenti & Mathews 1997a) – both in dominant group galaxies and in members of rich clusters – strongly suggests that all large ellipticals have retained part of the hot circumgalactic gas from their previous small group environment. The elliptical-dominated groups observed by Mulchaey et al. (1996) may be typical of the early development of most or all giant ellipticals. Some gas dynamical memory of these massive gaseous halos persists even after bright ellipticals enter cluster environments. As a bright galaxy moves deep into a large cluster, the pressure of hot gas in its outer atmosphere may be supplanted by the pressure of the hot diffuse cluster gas. In this manner the characteristic high temperature and positive dT/dr that are established within a few r_e may not be greatly altered even when gas in the outer galaxy is stripped away; NGC 4649, deep in Virgo, may be an example of this.

In the future it will be necessary to show that massive, extended halos of hot gas, similar to the one we require here, are an inevitable consequence of early galactic evolution. The prevailing consensus today is that a significant outflow of gas occurred at early times during galactic evolution, $t \lesssim 1$ Gyr. The high metallicity observed in hot diffuse cluster gas indicates that winds were indeed common in the earliest times, either from the large ellipticals or from the hierarchical subunits that later merged to form them. It is therefore unclear how to reconcile the existence of the large halo of hot gas we hypothesize here with these early galactic winds. The hot gas is likely to have been acquired by massive galaxies over a few or many Gyrs, not provided all at once as we have assumed. However, our initial investigations of models in which additional gas is supplied gradually over the Hubble time have not been encouraging; in general these models are much more complicated and less successful than the one we discussed here.

But none of these complications should detract from our main conclusion: inflowing circumgalactic gas may help resolve many difficulties that have plagued the subject of cooling flows in elliptical galaxies. The radial variation of gas temperature and density can now be understood. The long-standing problem of the enormous scatter in the L_x/L_B plot (e.g. Eskridge et al. 1995) may result from disproportionate allocations of hot halo gas in group ellipticals of similar L_B following tidal transfers of halo material from subordinate to group-dominant ellipticals (Mathews & Brighenti 1997). We may also understand why the ratio of iron abundance in the gas to that in the stars is so variable and often so small. Differing amounts of incoming circumgalactic hot gas, assumed to have low iron abundance, can dilute the iron produced by galactic stars and supernovae in varying amounts, leading to a variety of (often very low) hot gas iron abundances for galaxies of similar L_B. Unfortunately, this simple idea is not supported by the few observations that currently exist. Finally, the apparent circularity of x-ray images of large, rotating ellipticals may be difficult to understand without additional sources of gas since gas lost from the stars naturally produces easily visible x-ray disks out to $\sim r_e$ even in slowly rotating ellipticals (Brighenti & Mathews 1996). If circumgalactic gas flowing in from the outer parts of massive ellipticals has less specific angular momentum than the stars, the visibility of x-ray disks would be reduced.

We wish to thank Annibale D'Ercole for allowing

us to use a modified version of his Eulerian code in performing the calculations discussed here. Our work on the evolution of hot gas in ellipticals is supported by NASA grant NAG 5-3060 for which we are very grateful. In addition WGM is supported by a UCSC Faculty Research Grant and FB is supported in part by Grant ASI-95-RS-152 from the Agenzia Spaziale Italiana.

REFERENCES

Arimoto, N., Matsushita, K., Ishimaru, Y., Ohashi, T., & Renzini, A. 1997, ApJ, 477, 128

Athanassoula, E., Makino, J., & Bosma, A. 1997, MNRAS 286, 825

Awaki et al. 1994, PASJ 46, L65

Balbus, S. A. 1991, ApJ, 372, 25

Bertin, G. & Toniazzo, T. 1995, ApJ, 451, 111

Bertschinger, E. 1985, ApJS, 58, 39

Bode, P. W., Berrington, R. C., Cohn, H. N. & Lugger, P. M. 1994, ApJ 433, 479

Brighenti, F. & Mathews, W. G. 1996, ApJ, 470, 747

Brighenti, F. & Mathews, W. G. 1997a, ApJ 486, L83

Brighenti, F. & Mathews, W. G. 1997b, ApJ, (submitted)

Buote, D. A. & Fabian, A. C. 1997, MNRAS (in press)

Ciotti, L., D'Ercole, A., Pellegrini, S. & Renzini, A. 1991, ApJ 378, 380

David, L. P., Forman, W., & Jones, C. 1991, ApJ, 369, 121

David, L. P., Jones, C., Forman, W., & Daines, S. 1994, ApJ, 428, 544

Davis, D. S. & White III, R. E. 1996, ApJ, 470, L35

Dubinski, J. 1997, preprint (astro-ph/9709102)

Eskridge, P. B., Fabbiano, G., & Kim, D-W. 1995, ApJS, 97, 141

Faber, S. M., Tremaine, S., Ajhar, E. A., Byun, Y-I., Dressler, A, Gebhardt, K., Grillmair, C., Kormendy, J., Lauer, T. R., & Richstone, D. 1997, ApJ (in press)

Fabian, A. & Nulsen, P. E. J. 1977, MNRAS, 180, 479

Forman, W., Jones, C., David, L., Franx, M., Makishima, K., & Ohashi, T. 1993, ApJ 418, L55

Garciagomez, C., Athanassoula, E. & Garijo, A. 1996, A&A 313, 363

Gunn, K. F. & Thomas, P. A. 1996, MNRAS 281, 1133

Hattori, M. & Habe, A. 1990, MNRAS, 242, 399

Ishimaru, Y. & Arimoto, N. 1997, PASJ 49, 1

Jones, C., Stern, C., Forman, W., Breen, J., David, L., & Tucker, W. 1997, ApJ, (in press)

Irwin, J. A. & Sarazin, C. L. 1996, ApJ, 471, 683

Kim, D-W. & Fabbiano, G. 1995, ApJ, 441, 182

Loewenstein, M. 1989, MNRAS, 238, 15

Loewenstein, M. 1966, in *Cosmic Abundances*, eds. S. S. Holt & G. Sonneborn, ASP Conf. Ser. v 99, 393

Loewenstein, M. & Mathews, W. G. 1991, ApJ, 373, 445

Loewenstein, M. & Mushotzky, R. F. 1996, ApJ, 466, 695

Malagoli, A., Rosner, R. & Fryxell, B. 1990, MNRAS, 247, 367

Magrelli, G., Bettoni, D., & Galletta, G.1992, MNRAS, 256, 500

Mathews, W. G. 1989. AJ, 97, 42

Mathews, W. G. 1990, ApJ, 354, 468

Mathews, W. G. & Brighenti, F. 1997, ApJ, (in press).

Merritt, D. 1985, ApJ 289, 18

Mulchaey, J. S., Davis, D. S., Mushotzky, R. F., & Burstein, D. 1996, ApJ, 456, 80

Mushotzky, R., Loewenstein, M., Awaki, H, Makishima, K, Matsushita, K., & Matsumoto, H. 1994, ApJ, 436, L79

Raymond, J. C., Cox, D. P., & Smith, B. W. 1976, ApJ, 204, 290

Renzini, A., 1997, ApJ (in press).

Sarazin, C. L. & Ashe, G. A. 1989, ApJ, 345, 22

Serlemitsos, P. J., et al. 1993, ApJ, 413, 518

Stewart, G. C., Canizares, C. R., Fabian, A, C., & Nulsen, P. E. J, 1984, ApJ, 278, 536

Thomas, P. A. 1986, MNRAS, 220, 949

Thomas, P. A., Fabian, A. C., & Nulsen, P. E. J. 1987, MNRAS, 228, 973

Trinchieri, G., Fabbiano, G., & Canizares, C. R. 1986, ApJ, 310, 637

Trinchieri, G., Fabbiano, G., & Kim, D-W. 1997, A&A, 318, 361

Trinchieri, G., Kim, D-W., Fabbiano, G., & Canizares, C. R. C. 1994, ApJ, 428, 555

Turatto, M., Cappellaro, E., & Benetti, S. 1994, AJ, 108, 202

van der Marel, R. P. 1991, MNRAS, 253, 710

Vedder, P. W., Trester, J. J. & Canizares, C. R. 1988, ApJ, 332, 725

White, R. E. & Sarazin, C. L. 1987a, ApJ, 318, 612

White, R. E. & Sarazin, C. L. 1987b, ApJ, 318, 621

White, R. E. & Sarazin, C. L. 1988, ApJ, 335, 688

Fig. 1.— (a) Observations and our analytic fits to gas temperature (top) and density (bottom) for *Einstein* HRI (filled circles) and ROSAT (open circles) data; (b) *solid curve*: M_{tot}; *long-dashed curves*: stellar mass M_* of NGC 4472; *dot-dashed curves*: total mass of hot gas; (c) *solid curve*: total mass density ρ_{tot}; *long-dashed curves*: stellar mass density ρ_* with a horizontal cut at the core or break radius $r_b = 0.023 r_e$.

Fig. 2.— *top:* Filled circles and open circles are gas densities observed in NGC 4472 with *Einstein* HRI and ROSAT respectively. The line is the density variation determined by the standard model (Model STD) at time $t = 13$ Gyr. *bottom*: Temperatures observed by ROSAT are shown with errorbars and the radial dependence of gas temperature determined for the standard model at time $t = 13$ Gyr is shown as a solid line.

Fig. 3.— Plots of the dropout functions $\Delta_0(T)$ (solid curve) and $\Delta_1(T)$ (dashed curve) for the ROSAT bandpass.

Fig. 4.— Variation of density and temperature in the cooling flow model with mass dropout (Model DO) *top:* gas density; *bottom*: background gas temperature of remaining gas (light solid line) and the mean effective temperature including that of gas dropping out (heavy solid line). The density and temperature for NGC 4472 are shown for comparison.

Fig. 5.— Variation of density and temperature in the cooling flow model with non-uniform α_* (Model NUA) *top:* gas density; *bottom*: gas temperature. The density and temperature for NGC 4472 are shown for comparison.

Fig. 6.— Variation of density and temperature in the cooling flow model with non-uniform Λ (Model NUL) *top:* gas density; *bottom*: gas temperature. The density and temperature for NGC 4472 are shown for comparison.

Fig. 7.— Variation of density and temperature in cooling flow models with increased supernova rates (Models SN1 and SN2). *top:* gas density for model SN1 (SNu(t_n) = 0.25) (solid line) and for model SN2 (SNu(t_n) = 0.45) (dashed line); *bottom*: gas temperature for model SN1 (SNu(t_n) = 0.25) (solid line) and for model SN2 (SNu(t_n) = 0.45) (dashed line). The density and temperature for NGC 4472 are shown for comparison.

Fig. 8.— Variation of density and temperature in cooling flow models with additional gas at early times (Models EXG1 and EXG2). *top:* gas density for model EXG1 (normal α_*) (dashed line), for model EXG2 (α_* reduced by 2) (solid line), for model STD (dotted line) and for model EXG1:0 with no stellar gas contribution (dot-dashed line); *bottom*: gas temperature for model EXG1 (normal α_*) (dashed line), for model EXG2 (α_* reduced by 2) (solid line), for model EXG2 (α_* reduced by 2) (solid line), for model STD (dotted line) and for model EXG1:0 (dot-dashed line). The density and temperature for NGC 4472 are shown for comparison.

This 2-column preprint was prepared with the AAS LaTeX macros v4.0.

Table 1

GLOBAL PROPERTIES OF COOLING FLOW MODELS

Model	L_x [a] (10^{40} ergs s^{-1})	$\langle z_{\rm Fe}/z_{\rm Fe\odot}\rangle$ [b]	$M_{\rm hot}$ [a] (10^{10} M$\odot$)	$M_{\rm cold}$ [a] (10^{10} M$\odot$)
STD	19.54	1.03	0.62	6.58
DO	12.98	1.15	0.53	6.7[c]
NUA	29.13	0.78	0.76	7.77
NUL	8.70	0.97	0.73	6.38
SN1[d]	43.10	4.41	1.64	5.01
SN2[e]	7.66×10^{-4}	9.64	1.32×10^{-2}	–
EXG1	90.22	0.58[f]	4.62	7.34
EXG2[g]	49.14	0.85[f]	4.25	3.52
NGC 4472	45.6[h]	0.33[i]	3.5	-

[a]Within 100 kpc.

[b]Averaged over x-ray emissivity.

[c]Cold gas is distributed throughout inner galaxy.

[d]$\mathrm{SNu}(t_n) = 0.25$ SNu.

[e]$\mathrm{SNu}(t_n) = 0.45$ SNu.

[f]Initial gas has $z_{Fe} = 0.1 z_{Fe\odot}$.

[g]For EXG2 α_* is reduced by 2.

[h]From Eskridge et al. (1995) scaled to $D = 17$ Mpc.

[i]From Arimoto et al. (1997); see text for other values.

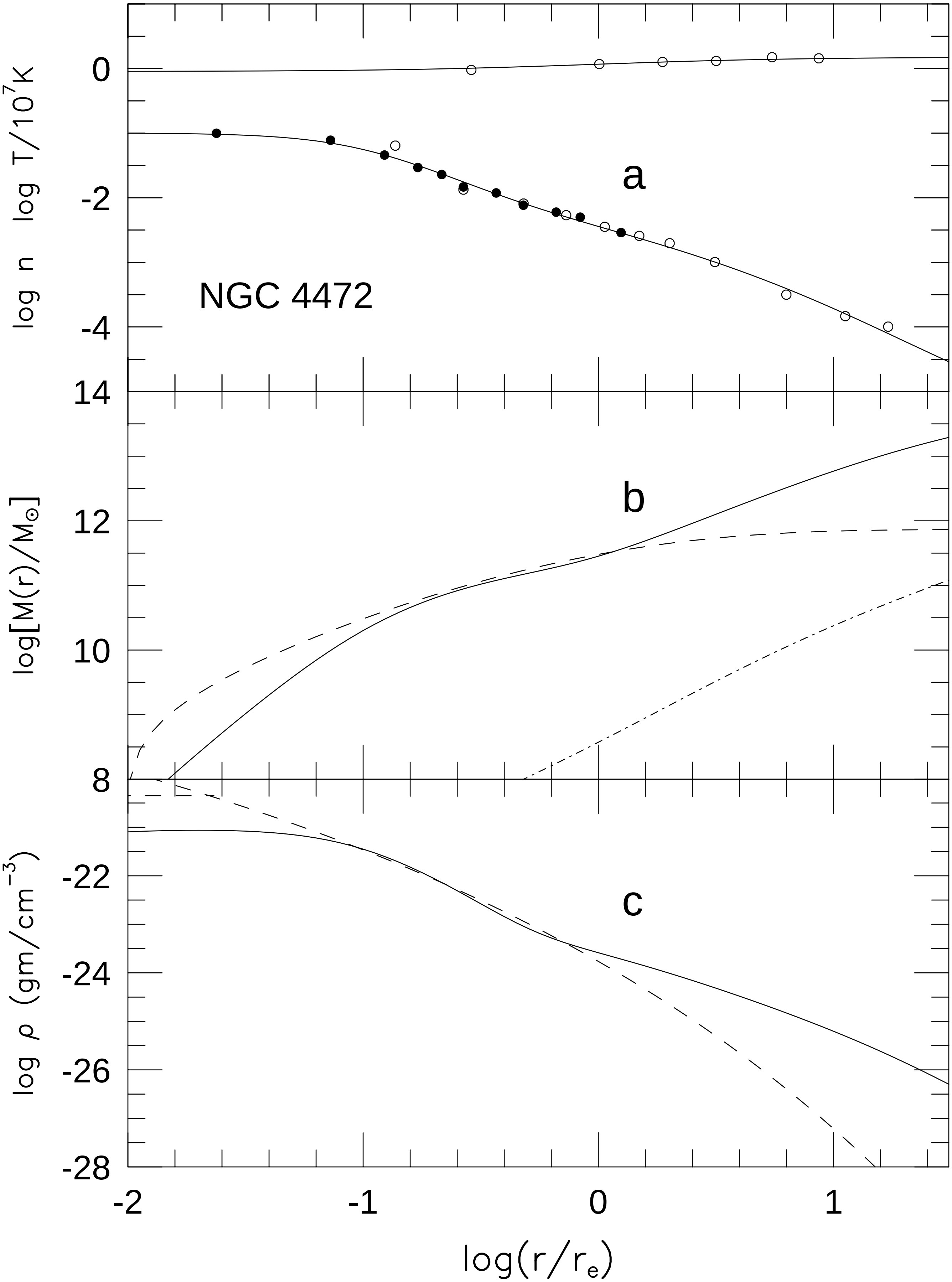
log n log T/10^7K
0
-2
-4
a
NGC 4472
14
12
10
8
log[M(r)/M⊙]
b
-22
-24
-26
-28
log ρ (gm/cm^-3)
c
-2
-1
0
1
log(r/r_e)

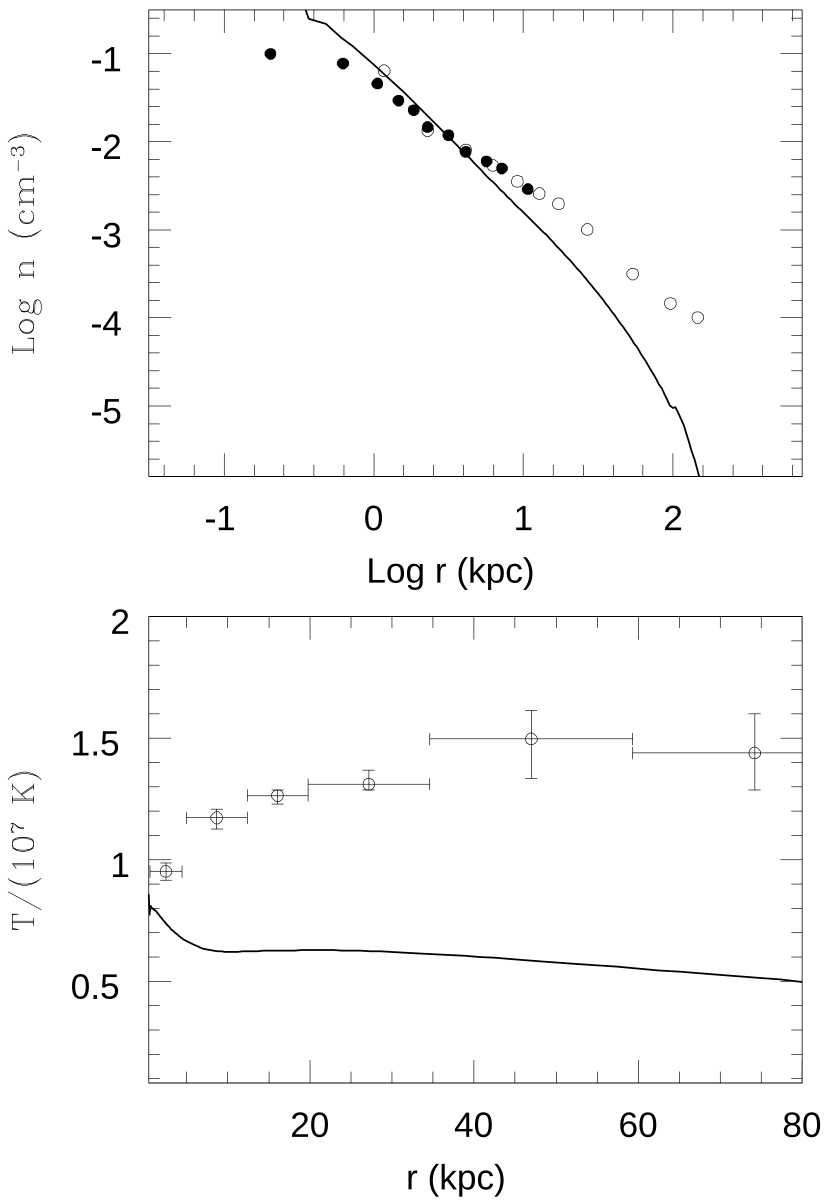

-1
-2
-3
-4
-5
Log n (cm^{-3})
-1
0
1
2
Log r (kpc)
2
1.5
1
0.5
T/(10^7 K)
20
40
60
80
r (kpc)

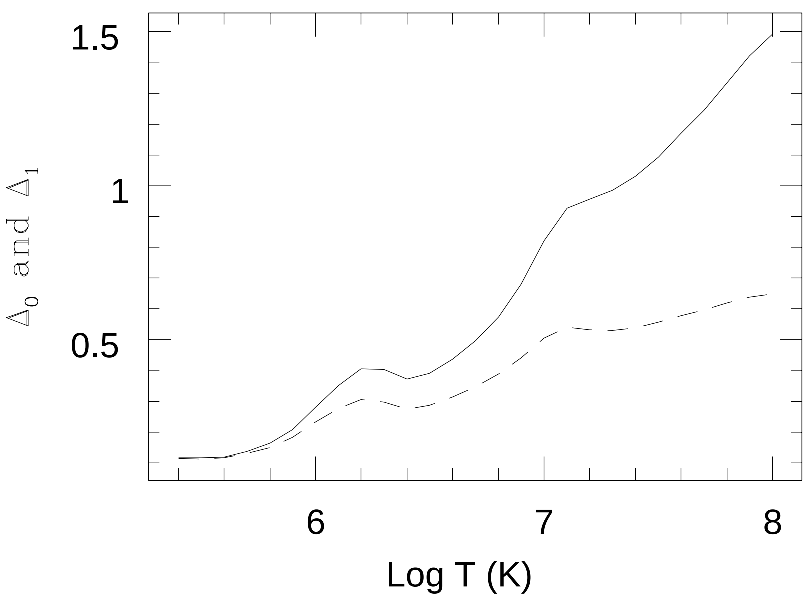

1.5
1
0.5
Δ_0 and Δ_1
6
7
8
Log T (K)

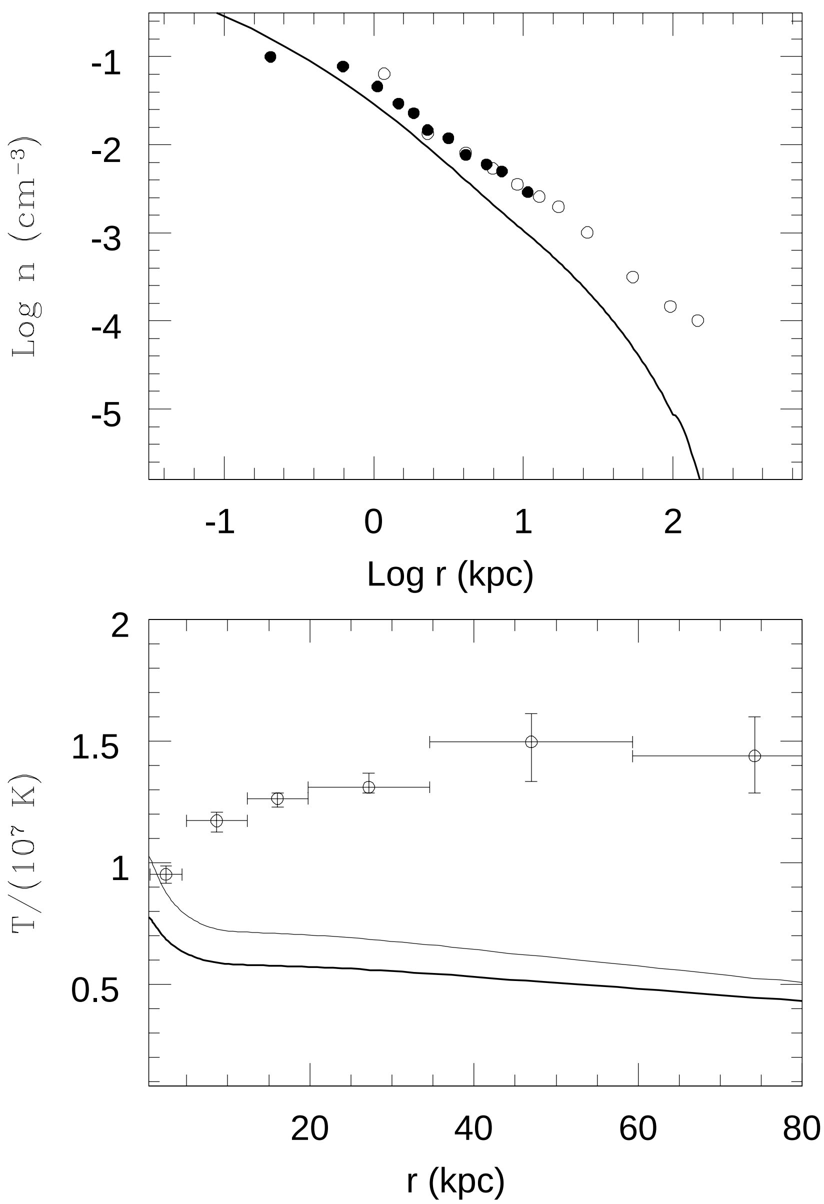

Log n (cm^{-3})
-1
-2
-3
-4
-5
-1
0
1
2
Log r (kpc)
T/(10^7 K)
2
1.5
1
0.5
20
40
60
80
r (kpc)

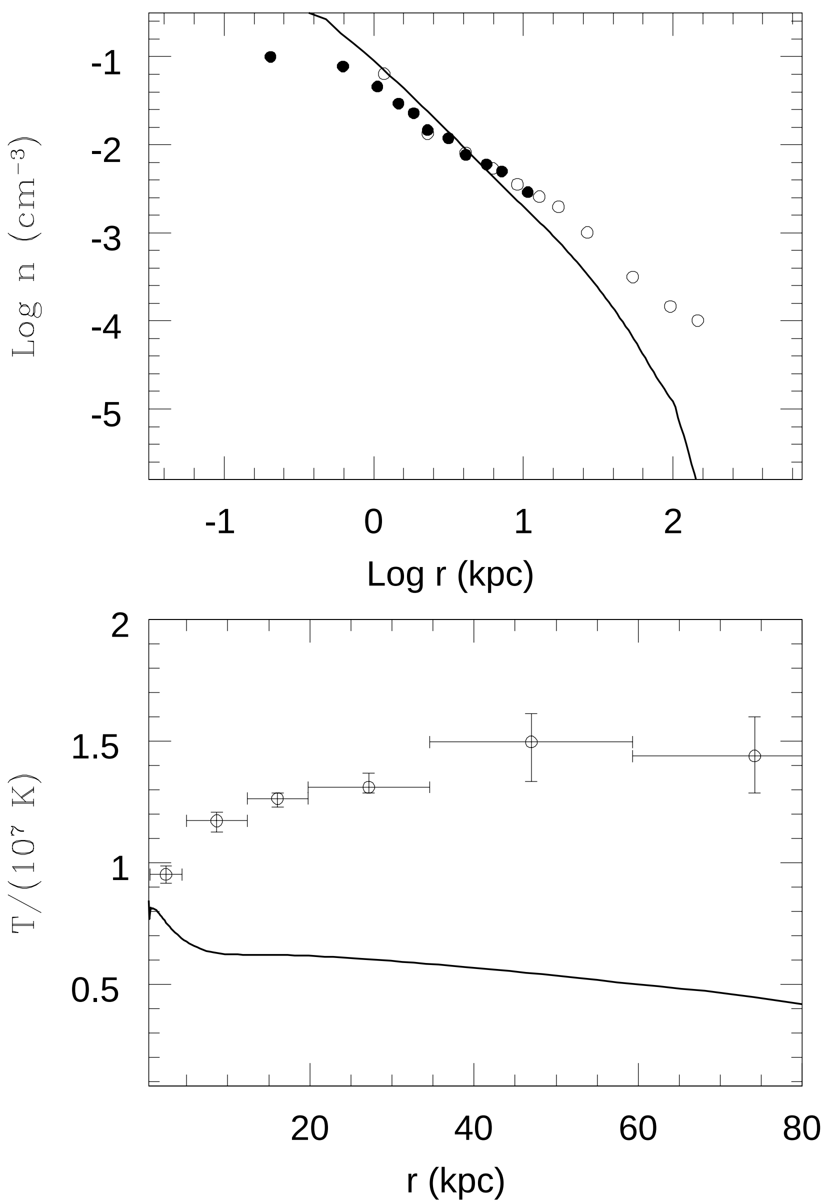
Log n (cm^{-3})
-1
-2
-3
-4
-5
-1
0
1
2
Log r (kpc)
T/(10^7 K)
2
1.5
1
0.5
20
40
60
80
r (kpc)

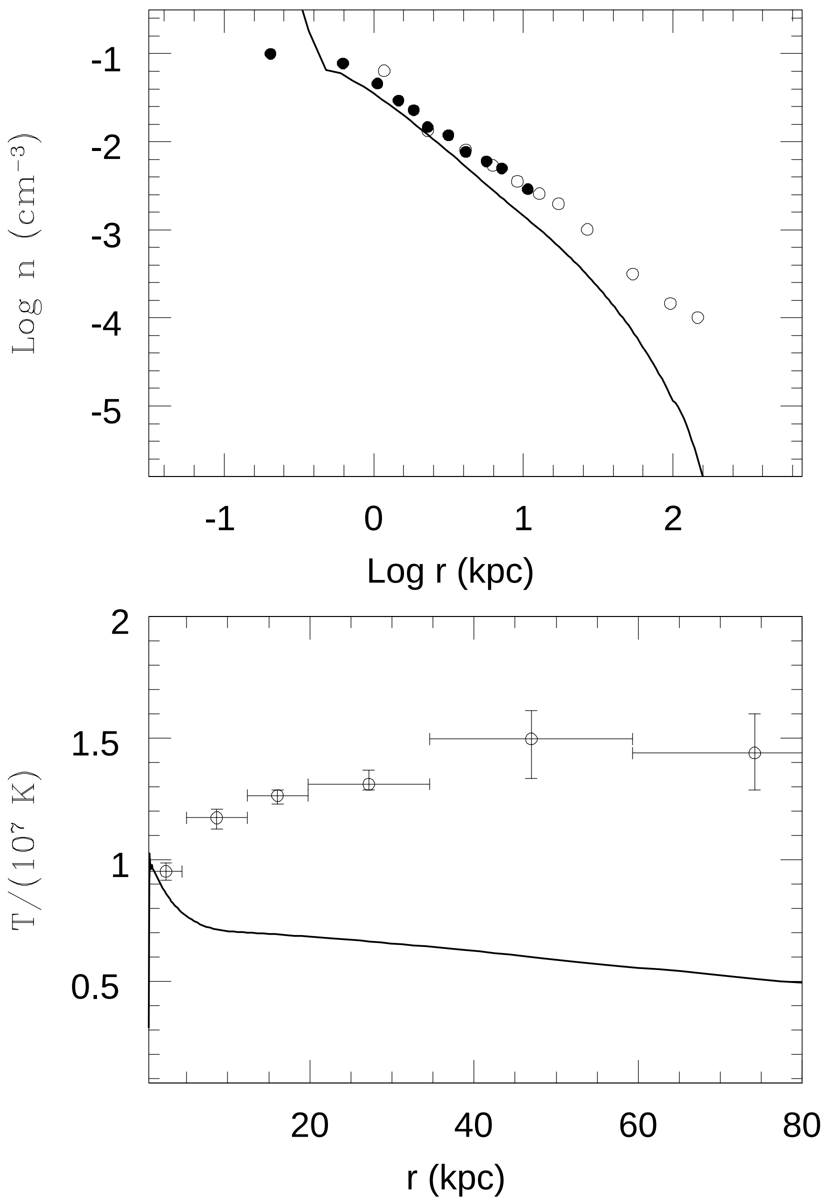

Log n (cm⁻³)
-1
-2
-3
-4
-5
-1
0
1
2
Log r (kpc)
T/(10⁷ K)
2
1.5
1
0.5
20
40
60
80
r (kpc)

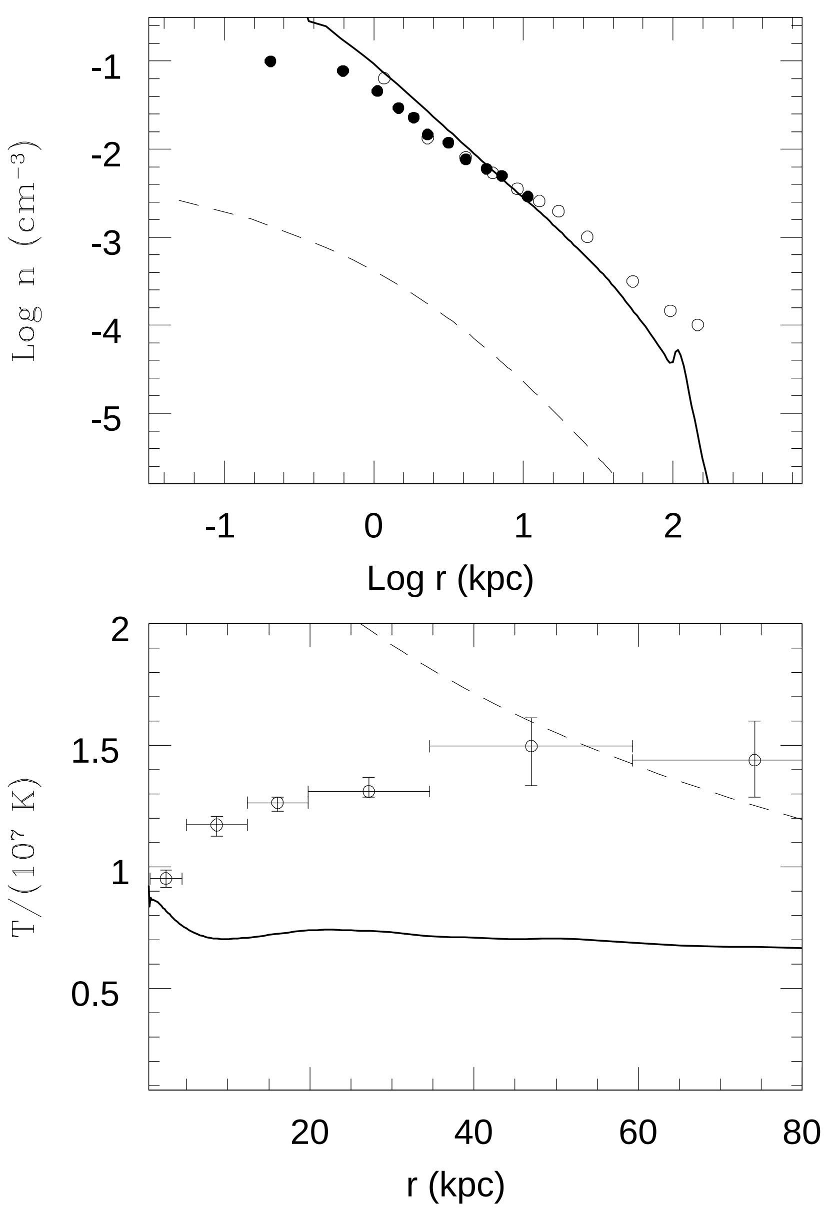

Log n (cm^{-3})
-1
-2
-3
-4
-5
-1
0
1
2
Log r (kpc)
T/(10^7 K)
2
1.5
1
0.5
20
40
60
80
r (kpc)

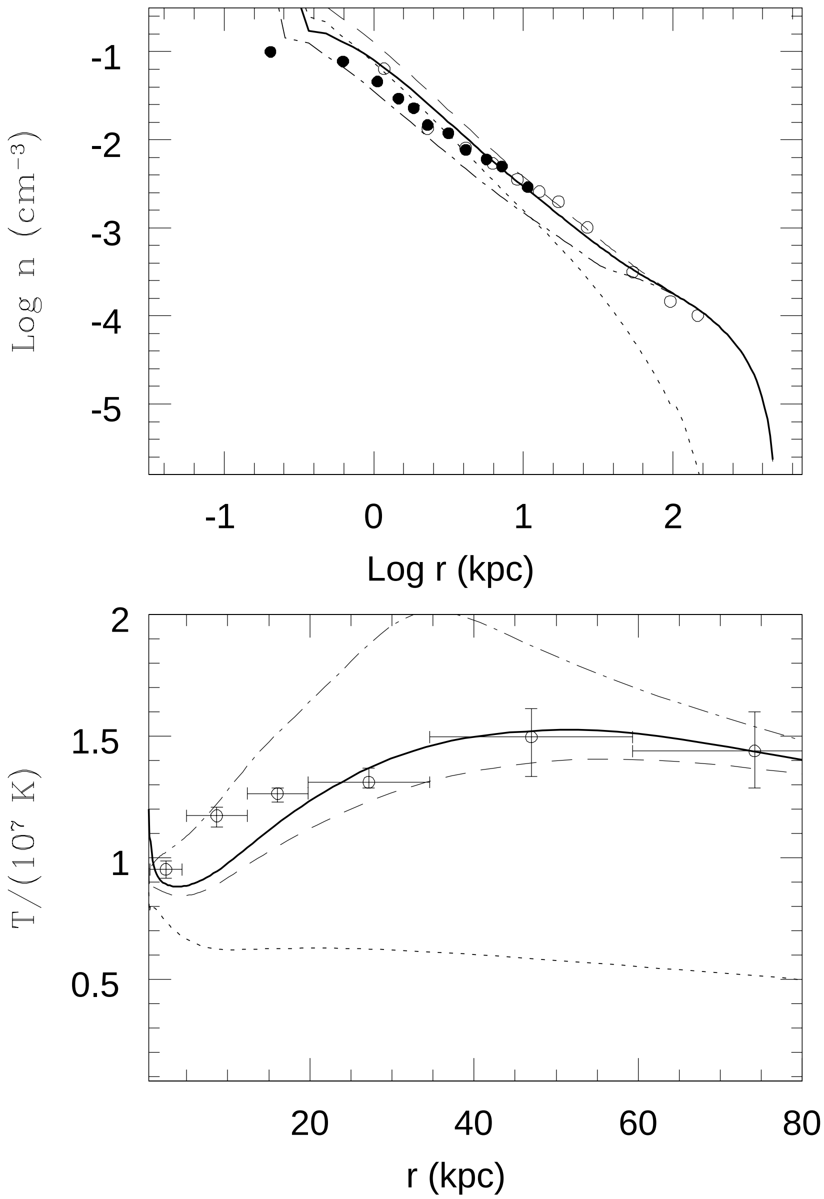

Log n (cm^{-3})
-1
-2
-3
-4
-5
-1
0
1
2
Log r (kpc)
T/(10^7 K)
2
1.5
1
0.5
20
40
60
80
r (kpc)